# Finite-Offset CRS stacking using Differential Evolution and Very Fast Simulated Annealing global optimization algorithms

João Carlos R. Cruz (IG/CPGF/UFPA) and German Garabito (DPET/UFRN)



## Abstract

By means of the hyperbolic traveltime approximation, the finite-offset Common Reflection Surface (FO CRS) method is capable to simulate arbitrary offset seismic sections by stacking prestack seismic data along paraxial traveltime surfaces. In order to reconstruct seismic reflection events in common-offset sections, the 2-D FO CRS traveltime approximation depends on five kinematic attributes (or CRS parameters) for each selected point of the seismic section. The main challenge of this method is to provide a computationally efficient data-driven strategy for accurately determining the best set of CRS parameters. For comparison, we apply two optimization strategies for simultaneously estimating the five parameters from prestack seismic data, the so-called Very Fast Simulated Annealing (VFSA) and the Differential Evolution (DE) global optimization algorithms. For one sample point of the common-offset section to be simulated, we compare the performance of both algorithms in respect to the efficiency and accuracy for estimating the five FO CRS parameters. We applied both optimization algorithms on real seismic data and showed the potential of them to enhance the reflection events in noisy data, even with very low signal-to-noise ratio.

## Introduction

Several macro-model velocity independent seismic stacking methods were introduced in the last years for simulating zero-offset sections from prestack seismic data. All these methods use a paraxial approximation of reflection traveltimes around the normal central ray. Zhang *et al.* (2001) developed a 2-D hyperbolic traveltime approximation for paraxial rays near to the finite-offset reflection central ray (Figure 1) as a function of five CRS-parameters. Two parameters at the source position, i.e. the start angle, $\beta_S$, and wavefront curvature, $K_2$, of a wave starting at the reflection point and three parameters at the receiver position, i.e. the emergence angle, $\beta_G$,and the wavefront curvatures $K_1$ and $K_3$ of two waves that start at the source and reflection point, respectively. The five parameters are used to define the stacking operator that approximates reflection events in the vicinity of a finite-offset central ray in midpoint and half-offset coordinates (Figure 2).

The finite-offset CRS stack method has been used for simulating finite-offset seismic sections in the common-shot, common-midpoint and common-offset data configurations (Bergler *et al*. 2002; Zhang *et al*. 2001 and 2002; Boelsen and Mann, 2005; Höcht *et al*. 2009). For example, summing up coherent events along the stacking operator and assigning the result to the time sample point of a finite-offset central ray, and repeating this operation for all points in a chosen common-offset section, yields the simulation of common-offset seismic data.

The FO CRS stack method needs very good estimates of the CRS-parameters from prestack data. The optimization problem of the FO CRS stack consists of searching for the best five CRS-parameters, in the sense of optimizing the coherence function, i.e. the objective function, without a priori information of the macro-velocity model, except of the near surface velocity.

Zhang *et al.* (2001) estimated the five finite-offset CRS-attributes by splitting the optimization problem into three steps and using simplified traveltime approximations for three seismic configurations, namely, common-midpoint (CMP), common-offset (CO) and common-shot (CS). They applied a grid search method to determine two coefficients in the CMP gathers $(a_{CMP}, b_{CMP})$, other two coefficients in the CO stacked gather $(a_{CO}, b_{CO})$, and the fifth coefficient $(b_{CS})$ in the CS gather. From these coefficients, for all samples of the target common-offset section are calculated the five CRS-parameters, and then the common-offset stacked section is simulated from multi-coverage prestack data.

Usually, the grid search is computationally very expensive method; on the other hand, the determination of the CRS attributes in several steps causes cumulative error, mainly in low fold and noisy datasets. Because the objective function of the finite-offset CRS stack method is multimodal and multidimensional, the optimization problem has no unique solution meaning that it is necessary to look for the global minimum. Garabito et al., (2016) presented the application of global optimization algorithm VFSA to search for simultaneously the five parameters of the 2-D FO CRS stack method.

The aim of this work is to analyze the performance of the VFSA algorithm in searching for the optimal five CRS-attributes and to simulate common offset sections from multi-coverage seismic data compared to another global optimization algorithm called Differential Evolution. For applications of the finite-offset CRS stack in synthetic and real data, we do not use any a priori information and the initial solution or starting point for global optimization was generated randomly.

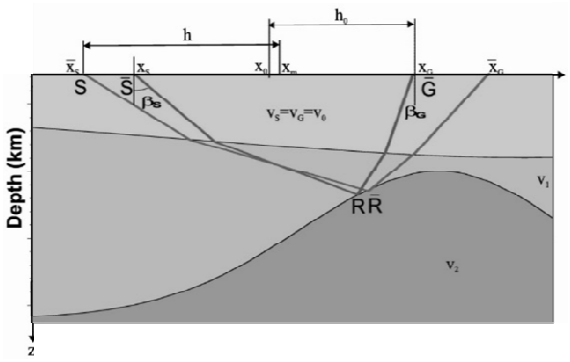


**Figure 1:** Central ray ($\mathbf{X_S\ R\ X_G}$) and paraxial ray ($\overline{\mathbf{X_S}}\ \overline{\boldsymbol{R}}\ \overline{\mathbf{X_G}}$) in earth stratified model.

**Theoretical aspects**

For a central ray that starts at *S* with initial velocity $v_s$ and start angle $\beta_S$, reflects at *R* in the subsurface, and emerges at the surface in *G* with final velocity $v_g$ and emergence angle $\beta_G$ (Figure 1); considering $v_s = v_g = v_0$, the traveltime of the finite-offset paraxial ray, so-called finite-offset CRS stacking operator, is expressed by (Zhang *et al*. 2001),

$$T_{CRS}^2 = \left[t_0 + \left(\frac{1}{v_0}\right)(a_1\Delta x_m + a_2\Delta h)\right]^2 + \left(\frac{t_0}{v_0}\right)[a_3 - a_4]\Delta x_m^2 - \left(\frac{t_0}{v_0}\right)[a_4 - a_5]\Delta h^2 + 2\left(\frac{t_0}{v_0}\right)[a_4 + a_5]\Delta x_m \Delta h. \quad (1)$$

by considering the relationships:

$a_1 = \sin\beta_G + \sin\beta_S$, $a_2 = \sin\beta_G - \sin\beta_S$, $K = 4K_1 - 3K_3$, $a_3 = K\cos^2\beta_G$, $a_4 = K_2\cos^2\beta_S$ and $a_5 = K_3\cos^2\beta_G$.

In Figure 2 the traveltime along the reflected central ray from *S* to *G* is $t_0$, while the source *S* and receiver *G* have horizontal coordinates, $x_S$ and $x_G$. The $x_0 = (x_G + x_S)/2$ and $h_0 = (x_G - x_S)/2$ are the midpoint and the half-offset of the central ray, respectively. The midpoint $x_m$ and half-offset $h$ correspond to the coordinates of the source and receiver positions of an arbitrary paraxial ray with finite-offset. The quantities $\Delta x_m = x_m - x_0$ and $\Delta h = h - h_0$ correspond to the midpoint and half-offset displacements of the paraxial ray $\bar{S}\bar{R}\bar{G}$ with respect to the coordinates of the central ray *SRG*.

By considering the same central ray *S* to *G* in the Figure 2, the wavefront curvature $K_1$ is obtained using the reflection/transmission law in a common-shot experiment and evaluated at the receiver position, while $K_2$ and $K_3$ are obtained by applying the transmission law for a hypothetical point source at the reflection point and evaluated, respectively, at the initial and final positions of the central ray in common-midpoint configuration.

In order to compare the finite-offset CRS stacking operator and the multicoverage ray theoretical traveltimes, we consider a central ray in the synthetic model in the lower part of Figure 2 constituted of two homogeneous layers over a half-space separated by curved and smooth interfaces with velocities $v_S = v_G = v_0$ = 1500 m/s, $v_1$ = 2600 m/s and $v_2$ = 3700 m/s, respectively.

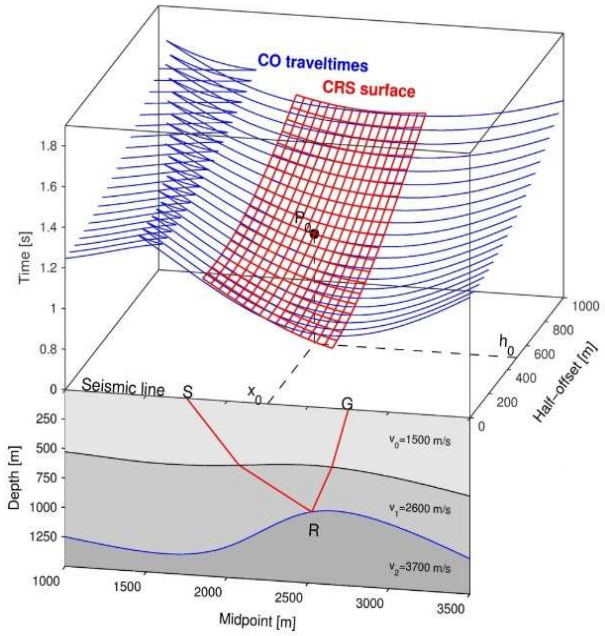


**Figure 2:** Constant velocity layered model and central ray SRG. The blue curves are the common-offset reflection traveltimes for the second reflector. The red curves define the FO CRS stacking operator referred to the point $P_0$.

By using the ray-tracing algorithm (Červený and Pšencik, 1988), we calculate the reflection traveltimes for several common-offset configurations and $K_1$, $K_2$ and $K_3$, as well as the angles $\beta_S$ and $\beta_G$ associated to a central ray . In the upper part of Figure 2, the blue curves represent the common-offset traveltimes of primary reflections associated to the second reflector and the red curves represent the CRS operator obtained by equation (1). Depending on the seismic configuration, we have the necessary adaptation of the finite-offset CRS approximation given by equation (1), i.e. for common-source , $\Delta x_m = \Delta h$, for common-midpoint , $\Delta x_m = 0$, for common-receiver, $\Delta x_m = -\Delta h$, and for common-offset, $\Delta h = 0$.

**FO CRS parameters optimization problem**

Because our objective is to simulate the common-offset seismic section from multicoverage seismic data, the optimization problem consists of finding the five finite-offset CRS parameters represented by the parameter vector $\mathbf{m} = (K_1, K_2, K_3, \beta_S, \beta_G)^T$. These five parameters are then used for calculating the finite-offset CRS stacking operator by equation (1).

The semblance function (Neidell and Taner, 1971) is a coherence measurement defined as the normalized ratio between the time-window accumulated energy after the summation of all traces and the time-window accumulated energy of all summed traces. It is expressed by:

$$S(\mathbf{m}; x_0, t_o) = \frac{1}{L}\frac{\sum_t\left(\sum_{i=1}^{L} U_{i,t(i)}\right)^2}{\sum_t\sum_{i=1}^{L} U_{i,t(i)}^2}. \quad (2)$$

The value $U_{i,t(i)}$ represents the amplitude of the seismic trace indexed by $i = 1,2, \dots L$, with *L* equals the number of seismic traces of the stacking surface. In the time window, the stack curve $t(i) = T_{CRS}(a_1, a_2, a_3, a_4, a_5; \Delta x_m^i, \Delta h_i)$ localizes the amplitudes according to finite-offset CRS traveltime approximation given by equation (1), where $\Delta x_m^i = x_m^i - x_0$ and $\Delta h_i = h_i - h_0$.

The finite-offset CRS optimization problem is to search-for the optimal parameter vector $\mathbf{m}$ which minimizes the the objective function, i.e. the negative of semblance function $S(\mathbf{m})$ in equation (2) for a triple $(x_0, h_0, t_o)$. It is a typical nonlinear, multidimensional, and multimodal optimization problem. For conflicting dip events the objective function is multimodal and it has the same number of local minima as the crossing events, but the event that has the highest energy will correspond to the global minimum. Therefore, although the objective function is multimodal, there is always a prominent global minimum especially when it is associated to only one reflection event.

In order to study the convergence behavior and selecting the control parameters of the VFSA and DE algorithms, a multi-coverage synthetic reflection dataset was generated using a ray tracing program of the SW3D Consortium, for the model in the lower part of Figure 2. The parameters of the dataset are: Length of the seismic line: from 0 to 5000m. First and last shots locations: 2000m and 5000m. Number of shots: 121. Number of receivers: 81. Interval between shots: 25 m. Interval between receiver stations: 25 m. Minimum and maximum offsets: from 0m to 2000m. Time sample interval: 4 ms. Record length: 2 sec. For the optimizations tests and simulating of a CO stacked section, in the dataset was applied a gain AGC and after it was added a random noise with signal-to-noise ratio 1.

**Very Fast Simulated Annealing (VFSA) algorithm**

Because it is computationally more efficient and able to solve multimodal and multivalued optimization problems, the VFSA was chosen to search-for the CRS kinematic attributes from prestack seismic data to simulate ZO seismic sections (Garabito *et al*. 2012; Minato *et al*. 2012). In the finite-offset CRS stack the determination of the five parameters is a highly nonlinear optimization problem. In Garabito et al., (2013) presented a detailed study of the control parameter of the VFSA algorithm for determining efficiently the five finite-offset CRS attributes. In addition, for a detailed description of the VFSA algorithm applied to FO CRS stacking, we address the readers to the paper Garabito, Cruz and Söllner (2016).

**Differential Evolution algorithm**

Let us consider an objective function $f(\mathbf{x})$ to be minimized with respect to the *D*-dimensional vector of parameters $\mathbf{x} = (x_1, x_2, x_3 \dots \dots, x_D)$. DE is based on a population with a size of *NP* (a positive integer), where each candidate solution is a *D*-dimensional vector,

$$\mathbf{x}_i = \left(x_{i,1}, x_{i,2}, \dots \dots \dots, x_{i,D}\right), \quad i = 1,2, \dots \dots \dots \dots NP. \qquad (3)$$

To initialize the population, the individuals are selected randomly within the boundary constraints of the search space,

$$x_{i,j}^0 = x_{i,j}^{min} + r_{i,j}\left(x_{i,j}^{min} - x_{i,j}^{max}\right),$$
$$i = 1,2, \dots . NP \quad \text{and} \quad \text{j} = 1,2, \dots \dots, D \qquad (4)$$

where $r_{i,j}$ is a random variable uniformly distributed in the interval [0, 1]. $x_{i,j}^{min}$ and $x_{i,j}^{max}$ are the lower and upper bounds of the *j*-th dimension of the search space, respectively. Each candidate solution is iteratively updated to search for the global minimum of $f(\mathbf{x})$ by three basic operators, namely, mutation, crossover, and selection (Barros *et al.*, 2015).

**Mutation operation**

Mutation is an operator by which a new solution vector is generated using the formula.

$$\mathbf{v}_i^G = \mathbf{x}_{r_1}^G + \boldsymbol{F}\left(\mathbf{x}_{r_2}^G - \mathbf{x}_{r_3}^G\right). \qquad (5)$$

The indexes $r_1, r_2, r_3 \in \{1,2, \dots NP\}$ are mutually distinct, chosen randomly, and different from the index *i*. The mutation scale factor ***F*** is a real and constant factor ∈ [0,2], which controls the length of the step given in the direction defined by $\left(\mathbf{x}_{r_2}^G - \mathbf{x}_{r_3}^G\right)$.

**Crossover operation**

Crossover operation is applied to each pair of the target vector $\mathbf{x}_{r_1}^G$ and its corresponding mutant vector $\mathbf{v}_i^G$ to generate a trial vector $\mathbf{u}_i^G$. In the basic version, DE employs the binomial (uniform) crossover defined as follows:

$$u_{ij}^G = \begin{cases} v_{ij}^G \ if \ r_j \le CR \ or \ j = j_{rand} \\ x_{ij}^G \qquad\qquad otherwise \end{cases}, \qquad j = 1,2, \dots \dots D. \qquad (6)$$

The crossover operation serves to enhance the diversity of the mutated parameter vectors, in the sense of making them cover a large region of the search space. In (6), the crossover rate $CR \in [0,1]$ is a user-specified constant, which controls the fraction of parameter values copied from the mutant vector and leads the algorithm to escape from local minimum.. $j_{rand}$ is a randomly chosen integer in the range [1,*D*].

**Selection operation**

The objective function value of each trial vector is compared to that of its corresponding target vector in the current population. If the trial vector $f(\mathbf{u}_i^G)$ has less or equal objective function value than the corresponding target vector $f(\mathbf{x}_i^G)$, the trial vector will replace the target vector and enter the population of the next generation. Otherwise, the target vector will remain in the population for the next generation.

The above three steps are repeated generation after generation, until some specific termination criteria are satisfied, as we can see in the flowchart in Figure 3.

**Control parameters of DE and VFSA**

The appropriate control parameters of a global optimization algorithm provide accurate results and reduced computational cost. In order to select control parameters and to study the performance of the DE and VFSA algorithms, we made tests in the noisy synthetic dataset generated for the model in the lower part of Figure 2. The tests are referred to the point $P_0$ corresponding to the reflection traveltime of the central ray depicted with red line, whose coordinates are $x_0 = 2250,\ h_0 = 500$ and $t_o = 1.140s$. The constant near surface velocity is $v_0 = 1500\, m/s$. Then, the selection of the control parameters for both algorithms was carried out through convergence runs and for discrete sets of the control parameters. For each independent run of the DE or VFSA algorithms searching the five FO-CRS attributes, the algorithm stops when it reaches 4000 function evaluations or when the global minimum is found even before reaching the maximum cost function evaluations.

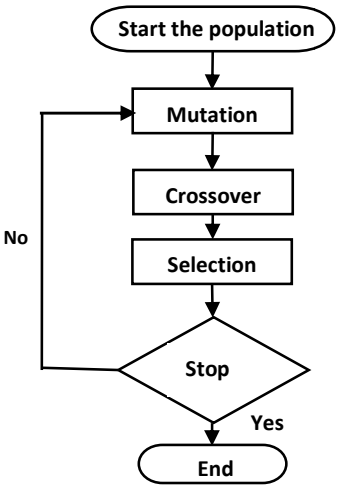


Figure 3: Flowchart of DE algorithm.

**DE parameters**

For DE algorithm the three control parameters are the population size $NP$, a constant integer that is chosen accordingly the dimension of the optimization problem; the crossover factor $CR\in$ [0,1] and the mutation scaling factor $F\in$ [0,2].

For fixed $CR = 0.8$, which is considered a good selection by means of previous tests, and for a bi-dimensional regular grid values of $NP$ and $F$, it was generated the performance surface shown in Figure 4a. By choosing the $NP = 25$ from the results shown in Figure 4a, for a bi-dimensional grid values of the $CR$ and $F$, it was generated the performance surface for DE algorithm in Figure 4b.

In both results, the smooth areas with higher objective function values correspond the best combination of control of parameters for DE algorithm to converge to the global minimum. In these areas the DE algorithm converges to the global minimum before reaching the maximum number of function evaluations. In the rugged areas with low and fluctuating values of the objective function, the algorithm stop when it reaches the maximum number of evaluations of the objective function. From these results, we choose the following best values for optimizing the five FO-CRS attributes: $CR = 0.8$, $F = 0.5$, $NP = 25$.

**VFSA parameters**

We follow the same procedure as used for the DE algorithm to select the control parameters for VFSA algorithm. The three control parameters of the VFSA are the initial temperature $T_0$, the cooling rate $C_i$ and the number of trials moves NT.

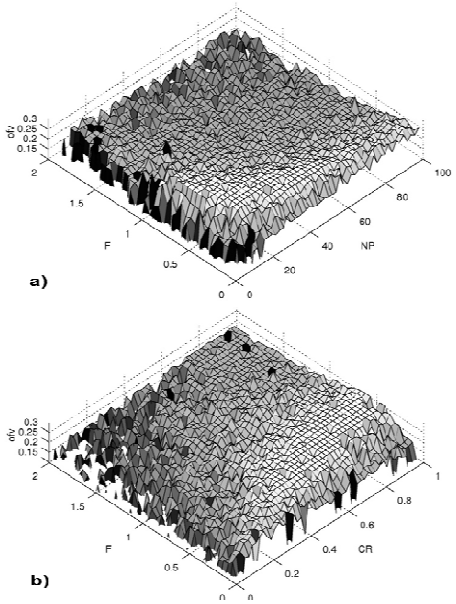


Figure 4: Performance surfaces of DE optimization algorithm: a) For fixed $CR = 0.8$ and b) for fixed $NP = 25$.

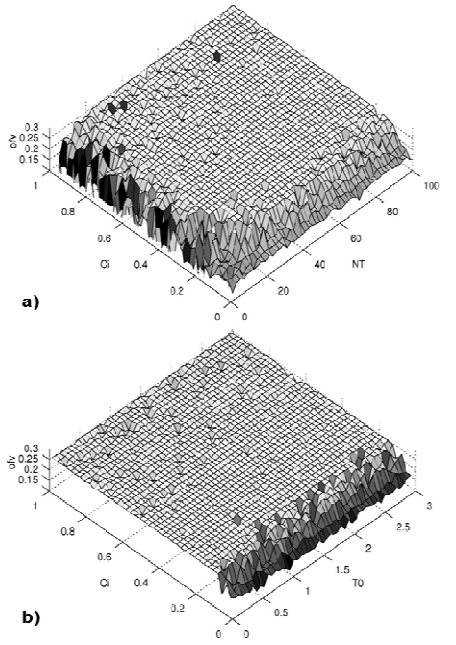


Figure 5: Performance surfaces of the VFSA algorithm: a) For fixed $NT = 50$ and b) for fixed $T_0 = 1.5$.

Through several tests of the VFSA algorithm optimizing the five FO-CRS attributes, we observed that the initial temperature does not affect significantly the performance of VFSA. Then, by fixing the initial temperature to $T_0 = 1.5$ for a regular grid vales of $C_i$ and $NT$, it was generated the performance surface for the VFSA algorithm shown in Figure 5a. The flat smooth areas are related with the best performance and efficiency of the optimization algorithm. From Figure5a, we observe that the NT is less sensitive and must be greater than 20, and then we choose $NT = 50$. Using this value and for a regular grid of $C_i$ and $T_0$, it was generated other performance surface shown in Figure 5b.

Both results show flat smooth areas, where the VFSA algorithm converge to the global minimum. In the flat areas with small fluctuations the algorithm decreases its performance and in the areas with high fluctuations the combinations of the control parameters are not appropriate. From both performance surfaces in Figures 5a and 5b, the VFSA parameters must be chosen in the intervals $C_i > 0.3$ and $C_i < 0.5$. From these results the best values are: $T_0 = 1.5$, $C_i = 0.4$, and $NT$=50. We emphasize that similar values of control parameters for VFSA were selected in Garabito et al (2017).

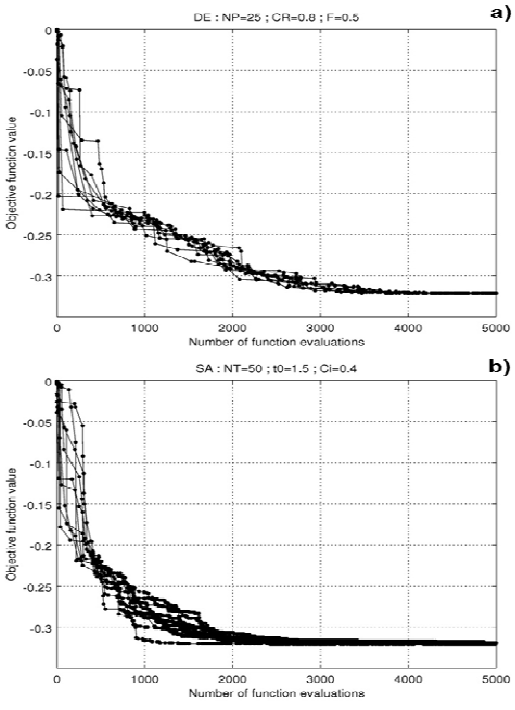


Figure 6: Convergence plots of the optimization algorithms to search the five FO CRS attributes: a) DE algorithm and b) VFSA algorithm.

In order to compare the performance of DE and VFSA algorithms to find the optimal solution for the five FO-CRS attributes, we perform the convergence tests using the same synthetic dataset and sample point $P_0$ of coordinates $(x_0 = 2250m, h_0 = 500m, t_0 = 1.140s)$. We applied the both algorithms using the control parameters selected before. Figure 6a shows the convergence curves for 10 single runs of the DE algorithm. Approximately after 3800 evaluations of the objective function the algorithm reaches the global minimum for all runs. The Figure 6b shows the progress of convergence for 10 single runs of the VFSA algorithm. Approximately after 2900 evaluations of the objective function the algorithm reaches the global minimum.

These results reveals that the DE is effective, but much slower than VFSA. Because the VFSA reaches the global minimum faster, we can see it as efficient. As the VFSA converge to the global minimum faster, we can say that it is efficient, even though, after 2900 evaluations, some runs reach very close to the global minimum.

In Table 1, we show the exact and estimated values of the five FO-CRS attributes. The exact values are calculated by ray tracing and the estimated values are the average of 10 runs of the DE and VFSA algorithms. The DE algorithm has the lowest value of the objective function and, as expected, the VFSA algorithm due to the small-scale fluctuation around the global minimum has a slightly higher value. For three attributes $(\beta_g, K_1, K_3)$, the DE relative errors are slightly smaller in comparison with the VFSA errors.

| | $\beta_s$ | $\beta_g$ | $1/K_1$ | $1/K_2$ | $1/K_3$ | Coher. |
|---|---|---|---|---|---|---|
| Ray tracing | -30.98 | 11.55 | 1346.3 | -2462.9 | 1152.8 | |
| DE | -31.03 | 11.26 | 1445.5 | -2275.9 | 1337.0 | -0.321 |
| VFSA | -30.99 | 11.19 | 1518.2 | -2414.1 | 1424.5 | -0.319 |
| DE error (%) | 0.151 | 2.549 | 6.861 | 8.219 | 8.096 | |
| VFSA error (%) | 0.039 | 3.176 | 11.324 | 2.023 | 11.25 | |

Tabela 1: FO-CRS parameters calculated by raytracing and by DE and VFSA algorithms.

## APPLICATION IN LAND SEISMIC DATA

One of main application of the FO-CRS stacking is to enhance common-offset seismic data for using in migration process. In the following example, we applied it using the VFSA and DE global optimization to real land seismic data from Tacutu Basin, Northern Brazil. We use the seismic line 50-RL-87 acquired in the early 80's with a low fold (12 traces). The dataset was submitted to the following preprocessing: geometry, trace edition, static correction, amplitude correction, coherent noise attenuation, deconvolution, time-variant spectral whitening, velocity analysis, residual statics correction. The output of the flow is the input for the FO-CRS stack method. In Figure 7 is the common-offset section of 1000m extracted from the pre-processed dataset. The DE and VFSA optimization algorithms used the same control parameters as in the previous convergence studies. The CO sections simulated by the FO-CRS stack method using the DE and VFSA are shown in Figure 8a and 8b, respectively. Both results show great enhancement of the reflection seismic events in comparison to the original section (Figure 7). With some effort, it can be seen that the CO section obtained with DE algorithm introduces small improvements in some parts of the section. However, it is also observed that the linear coherent noise is highlighted in the DE section.

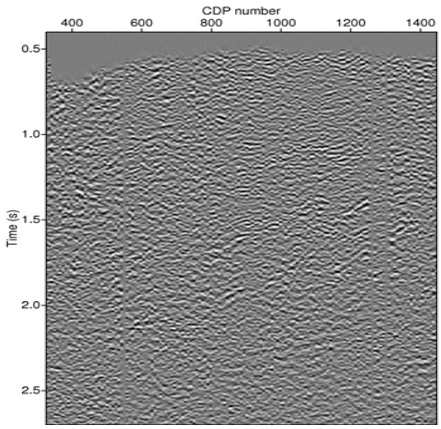


Figure 7: Original CO seismic section of 1000m extracted from processed prestack data.

**Conclusions**

In this paper we presented the fundamental concepts and practical aspects of the FO-CRS parameters determination by means of global optimization by using one single step strategy. For comparison, we made convergence tests for 10 runs using the DE and VFSA algorithms. We show that the DE algorithm is slower to converge to the global minimum, but the CRS attributes are determined with good precision. The VFSA algorithm converges more quickly, but the final parameters values show small-scale fluctuations around the optimal values. By applying to real land seismic data, both algorithms presented a very good performance and no significant differences are observed.

**Acknowledgments**

We thank Parnaiba Gás Natural S.A. for supporting the seismic imaging research project being developed at UFRN and UFPA for supporting the first author.

**References**

Barros, T.; Ferrari R.; Krummenauer R. and Lopes R., 2015. Differential evolution-based optimization procedure for automatic estimation of the common-reflection surface traveltime parameter. Geophysics, Vol. 80(6), WD189-WD200.

Bergler, S.,Mann, J., Höcht, G.and Hubral, P., 2002. The Finite-Offset CRS stack:an alternative stacking tool for subsalt imaging. 72nd Annual Internat. Mtg., Soc. Expl. Geophys., Expanded Abstracts.

Boelsen, T., Mann, J., 2005a. 2D CO CRS stack for OBS and VSP data and arbitrary top-surface topography. EAGE 67th Conference and Technical Exhibition, P181.

Cervený, V., Psensik, I., 1988. SEIS88, Ray tracing program package. Charles University, Prague, Tschech Republic.

Garabito, G., Cruz, J. C. R., Hubral, P., Costa, J., 2001. Common reflection surface stack by global optimization. 71th Annual Internat. Mtg., Soc. Expl. Geophys. Expanded Abstracts.

Garabito, G., Söllner, W., and Cruz, J.C., 2009, Macro-model independent migration to zero offset (CRS-MZO), In Extended abstracts, 71st EAGE Conference & Exhibition.

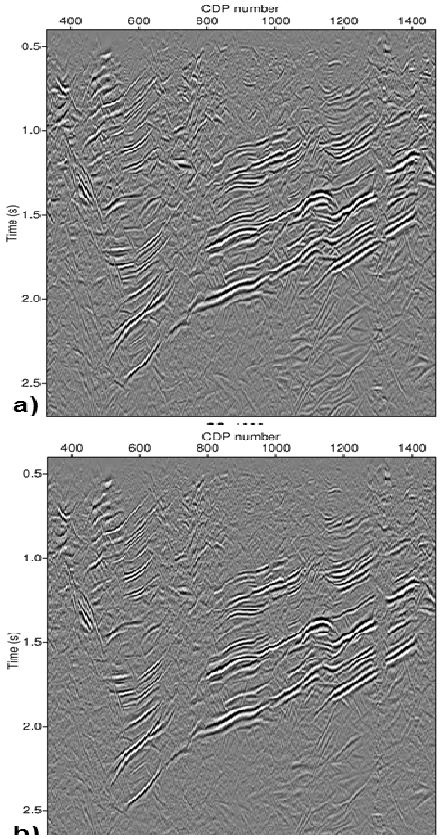


Figure 8: Enhanced CO section simulated by FO CRS stack using: a) DE algorithm and b) VFSA algorithm.

Garabito, G., Chira-Oliva P., Cruz, J. C. R., 2011. Numerical analysis of the common-reflection-surface traveltime approximation. J. Appl. Geophys., 74, 89-99.

Garabito, G., Stoffa, P. and Soellner, W., 2013. Global optimization of the common-offset CRS-attributes: Synthetic and field data application. Expanded Abstracts of the 13th. Cong. of Brazilian Geophysical Society, Brazil.

Garabito, G.; Cruz, J. C. R. and Söllner, W., 2016. Finite-offset common reflection surface stack using global optimization for parameter estimation: a land data example. Geophysical prospecting, doi:10.1111/1365-2478.12472.

Minato, S., Tsuji, T., Matsuoka, T., Nishizaka, N., Ikeda, M., 2012. Global optimization by simulated annealing for common reflection surface stacking and its application to low-fold marine data in Southwest Japan. Exploration Geophysics, 43, 59-69.

Neidell, N. S. and Taner, M. T., 1971. Semblance and others coherence measures for multichannel data. Geophysics, 36, 482-497.

Zhang, Y., Bergler, S., Hubral, P., 2002. Model-independent Travel-time Attributes for 2-D, Finite-offset Multicoverage Reflections. Pure and Applied Geophys. 159, 1–16.

Zhang, Y., Bergler, S., Tygel, M., Hubral, P., 2001. Common-Reflection-Surface (CRS) stack for common-offset. Geophys. Prospect., 49, 709–718.